Global Change Biology (2004) **10,** 1223–1239, doi: 10.1111/j.1365-2486.2004.00807.x

# Sensitivity of a dynamic global vegetation model to climate and atmospheric $CO_2$

STEFAN GERBER*, FORTUNAT JOOS* and I. COLIN PRENTICE†‡
*Climate and Environmental Physics, Physics Institute, University of Bern, Sidlerstrasse 5, CH-3012 Bern, Switzerland, †Max Planck Institute for Biogeochemistry, Winzerlaer Str. 10, D-07745 Jena, Germany, ‡QUEST, Department of Earth Sciences, University of Bristol, UK

**Abstract**

**The equilibrium carbon storage capacity of the terrestrial biosphere has been investigated by running the Lund–Potsdam–Jena Dynamic Global Vegetation Model to equilibrium for a range of $CO_2$ concentrations and idealized climate states. Local climate is defined by the combination of an observation-based climatology and perturbation patterns derived from a $4\times CO_2$ warming simulations, which are linearly scaled to global mean temperature deviations, $\Delta T_{glob}$. Global carbon storage remains close to its optimum for $\Delta T_{glob}$ in the range of $\pm 3\,^{\circ}C$ in simulations with constant atmospheric $CO_2$. The magnitude of the carbon loss to the atmosphere per unit change in global average surface temperature shows a pronounced nonlinear threshold behavior. About twice as much carbon is lost per degree warming for $\Delta T_{glob}$ above $3\,^{\circ}C$ than for present climate. Tropical, temperate, and boreal trees spread poleward with global warming. Vegetation dynamics govern the distribution of soil carbon storage and turnover in the climate space. For cold climate conditions, the global average decomposition rate of litter and soil decreases with warming, despite local increases in turnover rates. This result is not compatible with the assumption, commonly made in global box models, that soil turnover increases exponentially with global average surface temperature, over a wide temperature range.**

*Keywords:* carbon dioxide, $CO_2$, dynamic vegetation model, global warming, terrestrial biosphere, terrestrial carbon storage

*Received 20 November 2003; revised version received and accepted 20 January 2004*

## Introduction

Increased atmospheric $CO_2$ concentrations caused by anthropogenic emissions are expected to lead to a large change in climate by the end of this century (Houghton *et al.*, 2001). The projected $CO_2$ concentrations depend on future emissions but they also depend on the ability of the ocean and the terrestrial biosphere to sequester carbon (Prentice *et al.*, 2001). An important point of reference for terrestrial (and oceanic) carbon uptake is the equilibrium capacity for carbon storage under a given atmospheric $CO_2$ concentration and climate regime (Meyer *et al.*, 1999), here termed equilibrium carbon storage capacity (ECSC). The global terrestrial biosphere will be close to its ECSC for carbon storage if climate and atmospheric $CO_2$ varies slowly compared with the typical time scales of terrestrial carbon overturning and in the absence of anthropogenic land use. For fast changes in climate and $CO_2$, such as the present anthropogenic perturbation, the terrestrial biosphere will be out of equilibrium with the atmospheric forcing. The ECSC can, however, be considered as a reference point towards which the biosphere is relaxing, as long as nonlinear interactions and/or irreversible thresholds do not dominate.

Terrestrial uptake and ECSC are governed by a range of processes and feedbacks between the physical climate system and the land biosphere (Prentice *et al.*, 2001). Increasing temperatures will tend to decrease carbon storage in soils by enhancing soil respiration rates (Trumbore *et al.*, 1996). Warmer conditions in high-latitude and other temperature-limited regions for plant growth, will stimulate additional plant growth

Correspondence: Fortunat Joos, Climate and Environmental Physics, Physics Institute, University of Bern, Sidlerstrasse 5, CH-3012 Bern, Switzerland, fax + 41 31 631 87 42, e-mail: joos@climate.unibe.ch

 

and carbon uptake. Increasing atmospheric $CO_2$ will tend to increase water use efficiency, photosynthesis, and, hence, carbon uptake. Changes in rainfall regimes or temperature stress might lead to forest dieback and carbon loss.

Previous studies have investigated the transient terrestrial carbon uptake under anthropogenic forcing by evaluating carbon emission scenarios in coupled climate–carbon cycle models (Cox *et al.*, 2000; Friedlingstein *et al.*, 2001; Joos *et al.*, 2001; Leemans *et al.*, 2002) or by running terrestrial models offline from the climate model under prescribed climate and $CO_2$ forcing (Cao & Woodward, 1998; Meyer *et al.*, 1999; Cramer *et al.*, 2001). The ECSC has been evaluated with spatially resolved terrestrial models for a few different climate states and $CO_2$ levels only (Melillo *et al.*, 1993; Meyer *et al.*, 1999; Cramer *et al.*, 2001). Lenton & Huntingford (2003) have recently estimated ECSCs for a range of climate and atmospheric $CO_2$ applying a simple two-box model of the terrestrial biosphere.

Here, the ECSC is systematically investigated by simulating the equilibrium carbon storage for a range of climate regimes and $CO_2$ levels applying the Lund–Potsdam–Jena Dynamic Global Vegetation Model (LPJ-DGVM) in a highly idealized experimental setting. The model is appropriate for such an analysis because its treatment of terrestrial carbon cycle processes is based on first principles of plant physiology and ecology and does not assume that key processes of interest, such as net photosynthesis, are uniquely optimized under the present climatic conditions.

## Model and methods

### *Model description*

The LPJ-DGVM (Sitch *et al.*, 2003) simulates photosynthesis, plant distribution, and competition of nine plant functional types (PFTs). The PFTs considered are tropical broad-leaved evergreen trees, tropical broad-leaved raingreen trees, temperate needle-leaved evergreen trees, temperate broad-leaved evergreen trees, temperate broad-leaved summergreen trees, boreal needle-leaved evergreen trees, boreal summergreen trees, $C_3$ grasses/forbs, and $C_4$ grasses. The plant distribution is based on bioclimatic limits for plant growth and regeneration. PFT-specific parameters govern competition for light and water among the PFTs. Dispersal processes are not explicitly modeled, and an individual PFT can invade new regions if its bioclimatic limits and competition with other PFTs allow establishment. Carbon is stored in seven PFT-associated pools, representing leaves, sapwood, heartwood, fine roots, a fast and a slow decomposing above-ground litter pool, and a below-ground litter pool; and two soil carbon pools for each gridcell, receiving input from the litter pools of all PFTs present. Photosynthesis is a function of absorbed photosynthetically active radiation, temperature, atmospheric $CO_2$ concentration, day length, canopy conductance, and biochemical pathway ($C_3$, $C_4$), using a form of the Farquhar scheme (Farquhar *et al.*, 1980; Collatz *et al.*, 1992), with leaf-level optimized nitrogen allocation (Haxeltine & Prentice, 1996a) and an empirical convective boundary layer parameterization (Monteith, 1995) to couple carbon and water cycles. The burning flux of carbon is calculated based on litter moisture content, a fuel–load threshold, and PFT-specific fire resistances (Thonicke *et al.*, 2001). Decomposition rates of soil and litter organic carbon depend on soil temperature (Lloyd & Taylor, 1994) and moisture (Foley, 1995). Soil temperature is calculated (Sitch *et al.*, 2003) from surface air temperature and follows the surface temperature annual cycle with a damped oscillation and a temporal lag. Temperature diffusivity depends on soil texture and soil moisture. The spatial resolution is set here to $3.75^\circ \times 2.5^\circ$.

### *Model input and experimental setup*

The model is driven by monthly temperature, precipitation and cloud cover and by atmospheric $CO_2$. The climate input consists of a monthly climatology (Leemans & Cramer, 1991; Cramer *et al.*, 2001), overlaid with a 31-year interannual variability record obtained from a HadCM2 control run (Johns *et al.*, 1997). Changes in climate are expressed by spatial patterns of the perturbations in temperature, precipitation, and cloud cover. These patterns represent the first empirical orthogonal function (EOF) from a $4 \times CO_2$ scenario simulated with ECHAM3/LSG (Cubasch *et al.*, 1995; Hooss *et al.*, 1999; Voss & Mikolajewicz, 1999) (Fig. 1).

The climate variable $V$ in year $y$ and month $m$ at the location $x$ is determined as superposition of a baseline climate, interannual anomalies, and a climate perturbation:

$$V(x, y, m) = V_{\mathrm{clim}}(x, m) + \Delta V_{\mathrm{var}}(x, y, m) + \frac{\mathrm{EOF}_{\Delta V}(x)}{\sum_x \mathrm{EOF}_{\Delta V}(x)} \cdot r_{\Delta V} \cdot \Delta T_{\mathrm{glob}}. \quad (1)$$

$V_{\mathrm{clim}}$ represents the baseline climatology, $\Delta V_{\mathrm{var}}$ the interannual climate anomalies obtained from the HadCM2 simulation and repeated after each 31 years, $\mathrm{EOF}_{\Delta V}$ is the first EOF representing the spatial perturbation pattern for each variable, $\Delta T_{\mathrm{glob}}$ is the global mean surface temperature perturbation, and $r_{\Delta V}$ is a scaling factor ($r_{\Delta\mathrm{temperature}} = 1$, $r_{\Delta\mathrm{precipitation}} = 25.2\,\mathrm{mm\,yr^{-1}\,^\circ C^{-1}}$, $r_{\Delta\mathrm{cloud\ \ cover}} = -0.352\%\ ^\circ\mathrm{C}^{-1}$. The

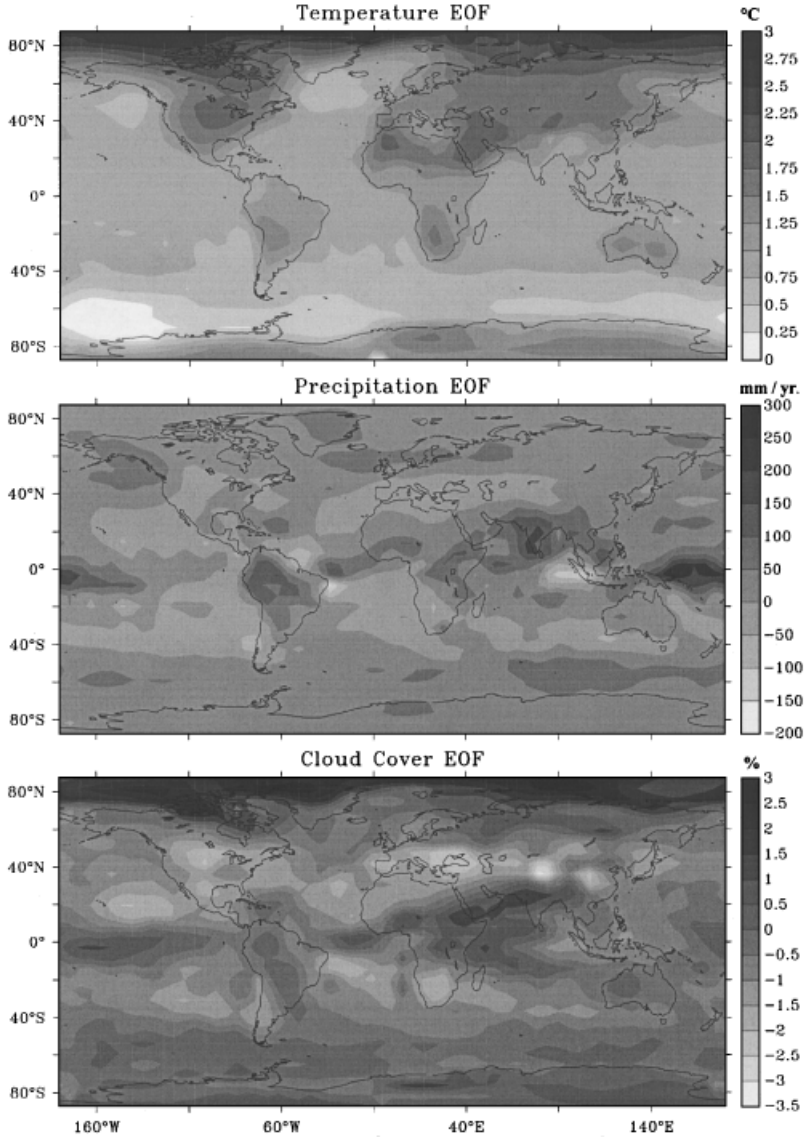


**Fig. 1** The spatial patterns of temperature (top), precipitation (middle), and cloud cover (bottom) perturbations associated with a change in global mean surface temperature of 1 °C as derived from a $4 \times CO_2$ simulation with the ECHAM3/LSG Atmosphere Ocean General Circulation Model (Hooss *et al*., 2001). These spatial perturbation patterns have been used to force the Lund–Potsdam–Jena dynamic global vegetation model in combination with a climatology.

scaling factors link the perturbations in precipitation and cloud cover to the global surface temperature perturbation. Interannual variability, $\Delta V_{var}$, is required to drive the fire routines of the model, however, results presented in the following do not depend critically on its exact specification.

Figure 1 shows the spatial climate change patterns. The ECHAM/LSG model yields the typical amplification of global warming in high northern latitude and in the interior of the Eurasian and North American continents where local temperature perturbations are well above the global average perturbation (Cubasch *et al*., 2001). Precipitation increases globally with global warming. Pronounced regional increases are simulated for tropical South America and the Indian subcontinent, whereas a decrease is obtained for the Mediterranean region and parts of western North America. Cloud cover changes are within a few percent.

In total, 246 simulations were carried out, where $\Delta T_{glob}$ was varied between $-10$ and $+10\,^{\circ}C$, and atmospheric $CO_2$ between 190 and 1000 ppm. It is intentional that this experimental setup represents a highly idealized situation. Changes in seasonality or in the distribution and frequency of extreme events are

not considered. Vegetation–climate feedbacks and changes in land ice cover, which might significantly alter the pattern of climate change, are likewise not considered. In reality, patterns also depend on the magnitude and sign of climate change and the type of radiative forcing. For each experiment, the LPJ-DGVM is spun up from bare ground for 1000 years under constant $CO_2$ and the specified climate. At year 400, soil carbon pool sizes are calculated analytically from annual mean litter inputs in order to reduce the time to reach equilibrium. The model is run for another 631 years. Then, averaged over the interannual cycle of the last 31 years, net biome production is well below 1‰ of the total inventory. Model results presented in the next sections are temporal averages over the last 31 years of each simulation.

## Results

### *Global ECSC and global carbon fluxes*

We begin our discussion by a factorial analysis to estimate the dependency of the ECSC on individual climate drivers and atmospheric $CO_2$. Changes in global carbon inventories in vegetation, soil, and litter, and changes in gross primary productivity (GPP), net primary productivity (NPP), heterotrophic respiration (RH), and the burning flux, are evaluated for changes in temperature, precipitation, cloud cover, and $CO_2$ (Table 1). The driving factors are varied individually and in various combinations. Points of reference are the preindustrial situation ($CO_2$: 280 ppm) and a world where atmospheric $CO_2$ is 490 ppm and global surface temperature is 2 °C above the preindustrial value. This combination of drivers corresponds to a midrange equilibrium climate sensitivity of 2.5 °C for a doubling of atmospheric $CO_2$ (Ramaswamy *et al.*, 2001).

The global ECSC increases from 2690 to 3460 Gt C when all drivers are changed. This increase by 770 Gt C is primarily the model's response to higher $CO_2$, whereas the combined changes in temperature, precipitation, and cloud cover without a $CO_2$ increase lead to a carbon loss of 130 Gt C. An increase in temperature alone leads to reduced carbon storage, primarily in soils and litter, in response to increased soil turnover rates and diminished carbon input. The carbon loss from soils and litter is almost an order of magnitude larger than the carbon loss from living vegetation. Carbon loss due to fire decreases as less litter is available for burning, although the rate of loss (loss per unit mass of

**Table 1** Changes in global terrestrial carbon pools and fluxes for simulations with LPJ-DGVM where driving factors were changed individually or combined for a nominal increase in global mean surface temperature of 2 °C and a $CO_2$ increase from 280 to 490 ppm

| Inventories | Vegetation (897) | Soil (1361) | Litter (434) | All pools (2693) |
|---|---|---|---|---|
| (a) $CO_2$ and climate | 480 | 148 | 140 | 768 |
| (b) $CO_2$ only | 423 | 316 | 179 | 918 |
| (c) Climate only | 47 | −147 | −31 | −131 |
| (d) 'Nonlinearities' $a-(b+c)$ | 10 | −21 | −8 | −19 |
| *Climate only* | | | | |
| (e) Temperature only | −32 | −194 | −69 | −295 |
| (f) Precipitation only | 85 | 10 | 20 | 115 |
| (g) Cloud cover only | 8 | 4 | 1 | 13 |
| (h) 'Nonlinearities' $c-(e+f+g)$ | −14 | 33 | 17 | 36 |
| **Fluxes** | **GPP (134)** | **NPP (66)** | **RH (59)** | **Fire (7.3)** |
| (a) $CO_2$ and climate | 62.8 | 29.0 | 27.0 | 2.0 |
| (b) $CO_2$ only | 50.1 | 24.6 | 21.0 | 3.6 |
| (c) Climate only | 7.9 | 2.3 | 3.2 | −0.9 |
| (d) 'Nonlinearities' $a-(b+c)$ | 4.8 | 2.1 | 2.8 | −0.7 |
| *Climate only* | | | | |
| (e) Temperature only | 0.5 | −1.3 | −0.4 | −0.9 |
| (f) Precipitation only | 7.4 | 3.2 | 3.3 | −0.1 |
| (g) Cloud cover only | −0.1 | 0.2 | 0.1 | 0.1 |
| (h) 'Nonlinearities' $c-(e+f+g)$ | 0.1 | 0.2 | 0.2 | 0.0 |

Units are Gt C for inventories and Gt C $yr^{-1}$ for fluxes. Inventories and fluxes for 280 ppm and preindustrial climate conditions are given in parentheses. GPP and NPP are positive for terrestrial carbon uptake from the atmosphere and RH and fire are positive for a carbon release into the atmosphere. LPJ-DGVM, Lund–Potsdam–Jena Dynamic Global Vegetation Model; GPP, gross primary productivity; NPP, net primary productivity; RH, heterotrophic respiration.

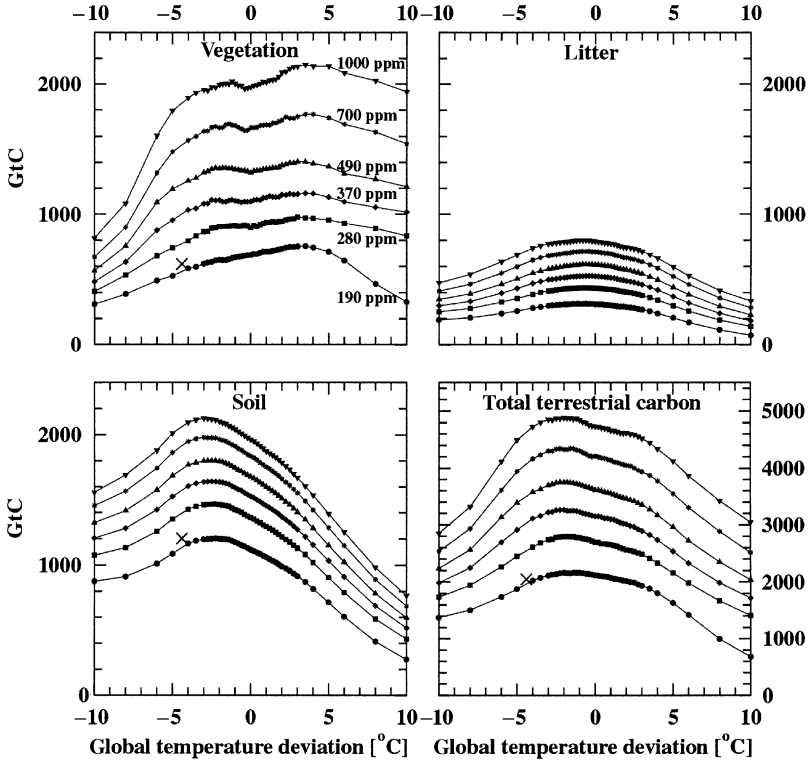


**Fig. 2** Simulated global carbon inventories of vegetation, litter, soil, and all reservoirs as a function of global average surface temperature and $CO_2$. Global temperature has been varied between −10 and +10 °C for six different levels of atmospheric $CO_2$ (190, 280, 370, 490, 700, and 1000 ppm; solid lines). Symbols denote individual simulations. The leave, sapwood, heartwood, and root compartments of all plant functional types are combined to calculate total vegetation carbon. Litter includes the fast and slow decomposing above ground and the below-ground litter compartments of all plant functional types, and soil carbon includes the fast and slow decomposing soil compartments. Note different scale for total terrestrial carbon. In the previous work (Joos *et al*., 2004), the Lund–Potsdam–Jena Dynamic Global Vegetation Model has been driven by the temperature and precipitation fields obtained with the National Centre for Atmospheric Research Climate System, Model Version 1.4, a coupled atmosphere–ocean general circulation model, for Last Glacial Maximum (LGM) boundary conditions ($CO_2$, ice sheet extent, sea level). Simulated values for this LGM simulation are shown by crosses.

litter) increases by about 4%. Changing precipitation alone leads to an increase in GPP and NPP, in response to reduced water stress, and consequently to an increase in global vegetation, litter, and soil carbon inventories. Changes in cloud cover alone have a minor impact on simulated storage.

Next, the global ECSC is investigated in a systematic way for a range of climate states and $CO_2$ concentrations (Fig. 2). This is done by varying the global mean temperature parameter, $\Delta T_{glob}$, between −10 and +10 °C at individual $CO_2$ levels. For each $CO_2$ level, temperature, precipitation, and cloud cover are varied locally following the patterns shown in Fig. 1 and the relationship given in Eqn (1).

The modeled carbon inventories show a strong sensitivity to atmospheric $CO_2$. The global ECSC is more than twice as large for a $CO_2$ concentration of 1000 than for 190 ppm and preindustrial climate. The sensitivity of the ECSC to climate variations, however, is qualitatively similar for $CO_2$ concentrations in the range of 190–1000 ppm (Fig. 2).

In simulations where $CO_2$ is kept constant, the modeled global carbon storage in vegetation decreases with cooling and increases slightly with a modest warming (Fig. 2). When $\Delta T_{glob}$ exceeds 3–4 °C, vegetation carbon starts to decline. Local maxima in vegetation carbon are found for $\Delta T_{glob}$ around −3 and +3 °C. These maxima are especially pronounced at high $CO_2$ concentrations and are related to the regional sensitivity of vegetation carbon to climate. A modest decrease $\Delta T_{glob}$ leads to an increase in tropical storage and little changes elsewhere, whereas a modest increase in $\Delta T_{glob}$ leads to an increase in high-latitude storage as further discussed in the next section. The simulated global carbon inventory in litter and soils shows a maximum at a global mean temperature deviation of −2 °C. It decreases rapidly with warming in response to accelerated soil respiration rates, despite a higher carbon

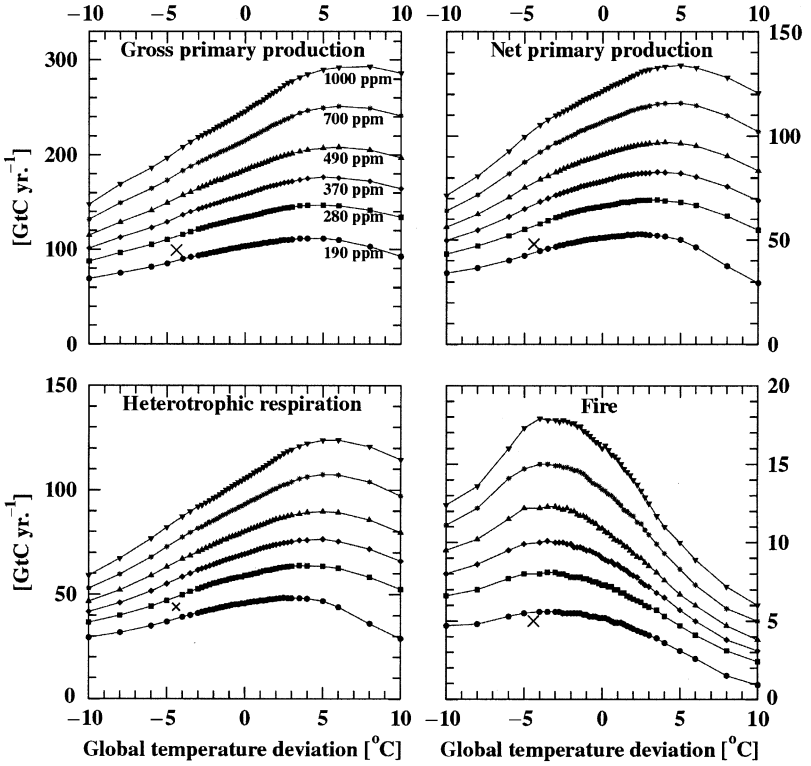


**Fig. 3** As Fig. 2, but for global carbon fluxes.

input from vegetation (Fig. 3; NPP). The sensitivity of global soil carbon storage to climate is much larger for positive $\Delta T_{glob}$ than for negative $\Delta T_{glob}$. This point will be further investigated in the section Global mean turnover rates and simple box models.

Simulated global ECSC is close to its maximum for present climate conditions and varies little for $\Delta T_{glob}$ between $-3$ and $+3\,^{\circ}C$. In this climate range, the sensitivity of the global terrestrial carbon inventory to climate change is small. On the other hand, global ECSC decreases for $\Delta T_{glob}$ below $-3\,^{\circ}C$ and above $+3\,^{\circ}C$. The magnitude of the net carbon flux to the atmosphere per unit change in global climate, $d(ECSC)/dT_{glob}$, shows a pronounced nonlinear threshold behavior. It undergoes large changes when crossing a global average surface temperature deviation of around $-3\,^{\circ}C$ and around $+3\,^{\circ}C$. Its value is around $170\,Gt\,C\,^{\circ}C^{-1}$ for glacial-type conditions, around $-75\,Gt\,C\,^{\circ}C^{-1}$ for $\Delta T_{glob}$ within $\pm 3\,^{\circ}C$, and around $-150\,Gt\,C\,^{\circ}C^{-1}$ above $3\,^{\circ}C$ and for an atmospheric $CO_2$ concentration of 370 ppm. $d(ECSC)/dT_{glob}$ increases with $CO_2$ for $\Delta T_{glob}$ below $\sim -3\,^{\circ}C$.

Simulated GPP increases almost linearly with $\Delta T_{glob}$ between $-10$ and $+3\,^{\circ}C$ (Fig. 3). The rate of increase is more pronounced for higher $CO_2$ concentrations. Simulated NPP shows similar characteristics, except that its maximum is at a slightly cooler climate. NPP is largely balanced by RH; simulated fire fluxes correspond to about 1/10 of the global NPP. The dependency of the global fire flux on $\Delta T_{glob}$ is similar to that of the litter carbon inventory. This suggests that modeled global fire fluxes are primarily governed by fuel availability.

### *Regional changes in carbon inventories and fluxes*

The distribution of different PFTs (Figs 4 and 5), terrestrial carbon inventories (Fig. 6) and carbon fluxes (Fig. 7) show distinct response patterns to climate change. The area populated by plants increases, and boreal, temperate, and tropical trees spread polewards with warming. Tropical trees are extremely restricted for a $\Delta T_{glob}$ of $-10\,^{\circ}C$ and are found as far north as 35°N for a $\Delta T_{glob}$ of $+10\,^{\circ}C$. Tree foliar projective cover (FPC, i.e. the fraction of the ground area covered by trees) increases in the tropics and subtropics with warming. The simulated maximum in tree FPC is found for present or somewhat warmer climate conditions between $\sim 35$ and 60°N. Growth becomes less viable for boreal tree types during hot summers and winter conditions are locally too harsh for temperate trees to establish in mid- to high latitudes, in particular in central Siberia and Canada. Grasses spread northward with warming and total FPC becomes close to 100% in

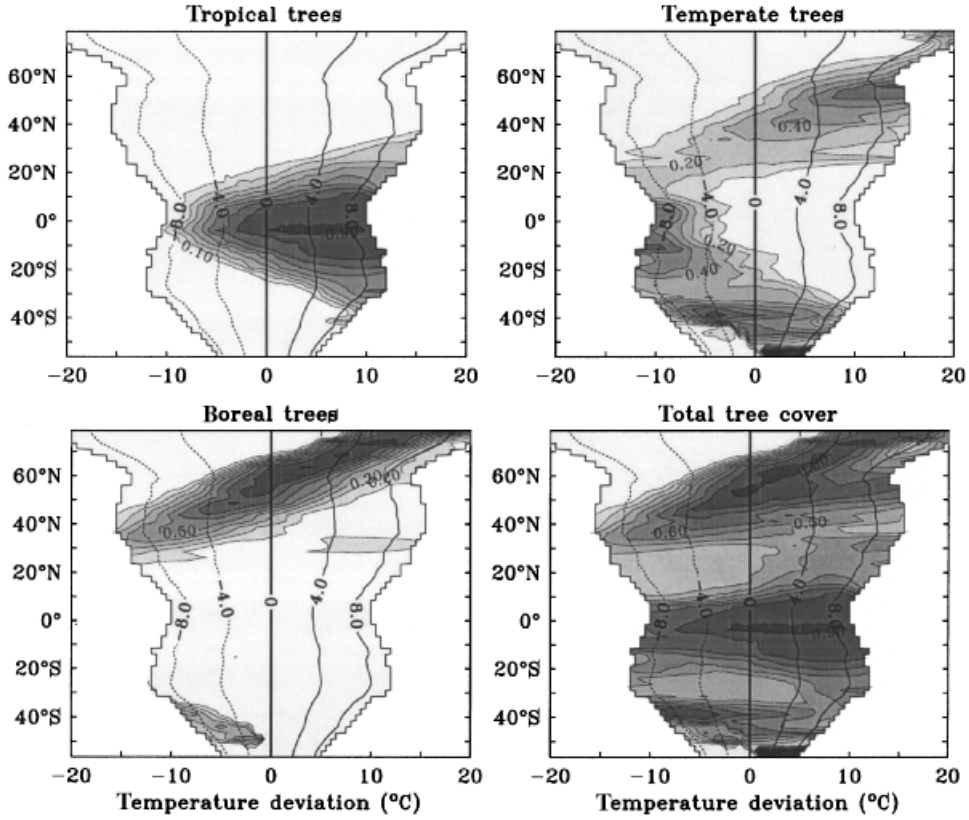


**Fig. 4** Simulated zonally averaged foliar projective cover for tropical, temperate, boreal, and all tree types as a function of latitude and the deviation in zonal mean land surface temperature. $CO_2$ concentration is set to 280 ppm. The near vertical lines relate the zonal mean land surface temperature deviations to the global surface temperature deviations for $\Delta T_{glob}$ of −10, −8, −4, 0, +4, +8, and +10 °C (For example, a $\Delta T_{glob}$ of 4 °C corresponds to a zonal mean land temperature change of about 9 °C at 80°N).

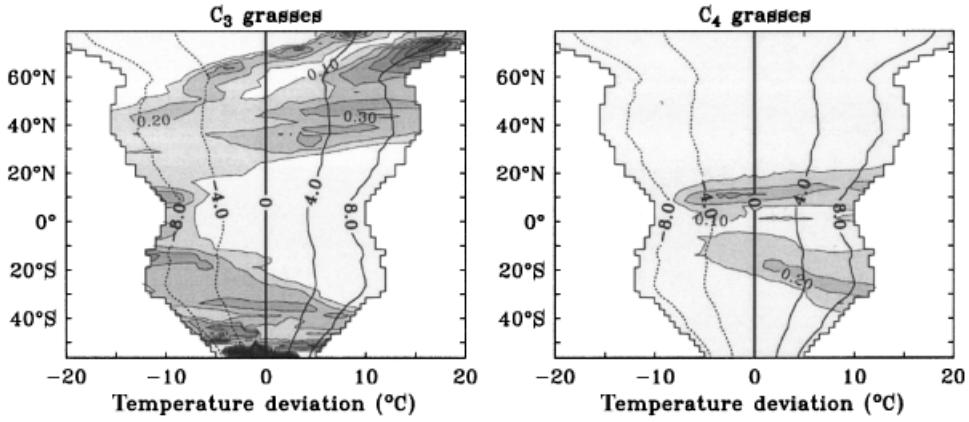


**Fig. 5** As Fig. 4, but for $C_3$ and $C_4$ grasses.

many regions. A similar response of plant distribution to warming was also found in transient scenario calculations with the same model (Joos *et al*., 2001).

The largest changes in carbon inventories and carbon fluxes are simulated in mid- to high latitudes. Poleward spreading of trees with warming leads to increased storage and fluxes reflected in the pattern north of 40°N (Figs 6 and 7). Except at high northern latitudes, total carbon storage, and carbon storage in soils and litter generally decreases with warming and increases with

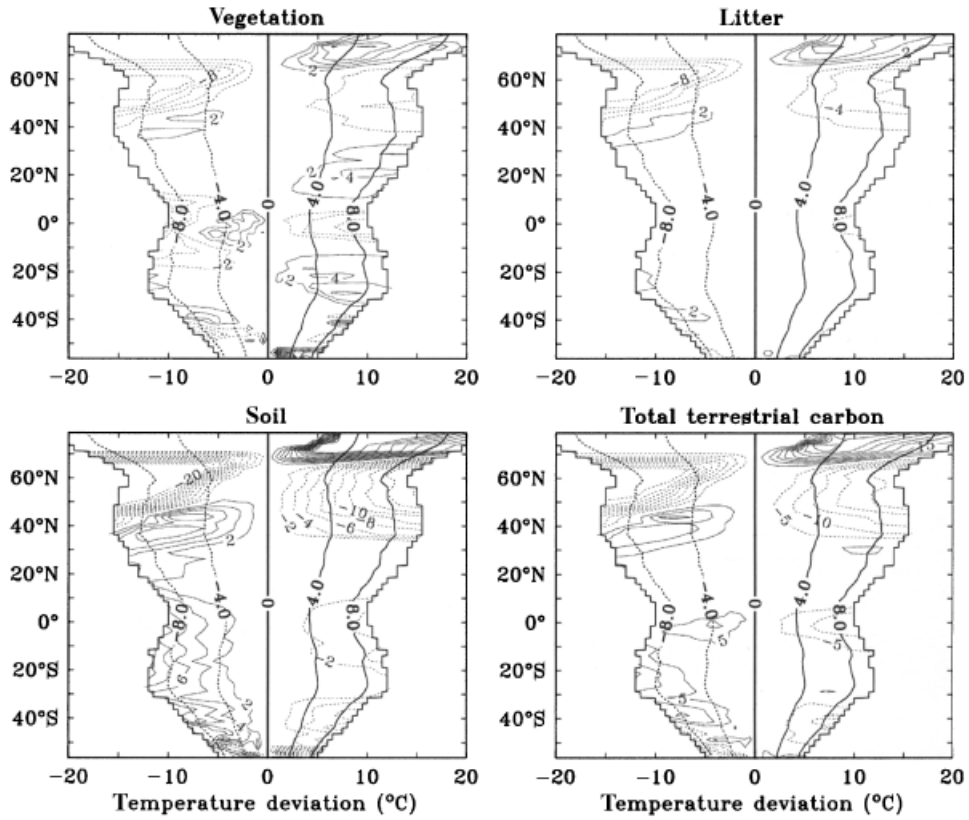


**Fig. 6** As Fig. 4, but for simulated changes in zonally averaged carbon storage in $kg\,C\,m^{-2}$. Positive changes are indicated by solid isolines and negative changes by dashed isolines.

cooling in response to altered organic matter decomposition rates. Simulated fire fluxes decrease as well with warming, as fuel availability decreases. Carbon storage in vegetation, productivity, and RH show a more latitude-dependent response to climate change. Around 40°N, vegetation carbon, NPP, RH, and fire fluxes undergo relatively small changes with climate. In contrast, the carbon stored in litter and soils decreases with warming at mid-latitudes in response to accelerated organic matter decomposition rates. In the subtropics, vegetation carbon and productivity increases with warming in particular in response to increased monsoonal precipitation, whereas total carbon storage remains relatively constant. In the tropics, vegetation and total carbon storages are highest for a climate that is a few degrees colder than today. Tropical vegetation carbon decreases with warming, despite a slight increase in tropical tree coverage. GPP decreases with warming climates principally because, other things being equal, the competition of $O_2$ with $CO_2$ for the Rubisco carboxylation site becomes stronger with increasing temperature, resulting in reduced quantum efficiency and reduced photosynthesis in the canopy as a whole.

### *The link between $CO_2$, global warming, the ECSC, and nitrogen requirements*

Next, we explore the coupling between changes in atmospheric $CO_2$, climate, and total carbon storage using the concept of radiative forcing and climate sensitivity (Ramaswamy *et al.*, 2001). The aim is to link changes in terrestrial carbon storage to a mutually consistent $\Delta T_{glob}$–$CO_2$ space.

The global radiative forcing by $CO_2$, RF($CO_2$), is taken to be logarithmically related to $CO_2$ (Myhre *et al.*, 1998):

$$\mathrm{RF}(CO_2) = 5.35\,\mathrm{W\ m^{-2}}\left(\ln\frac{CO_2}{CO_{2,0}}\right). \qquad (2)$$

Global average surface temperature change, $\Delta T_{glob}$, is linked to total radiative forcing by $CO_2$ and non-$CO_2$ agents, RF(all), and the climate sensitivity, $\Delta T_{2x}$, here expressed as the equilibrium change in global surface temperature for a nominal doubling of $CO_2$. At equilibrium holds:

$$\Delta T_{glob} = \frac{\Delta T_{2x}}{\mathrm{RF}(2x\mathrm{CO}_{2,0})}\mathrm{RF(all)}. \qquad (3)$$

Rearranging Eqn (3) yields the climate sensitivity divided by the relative contribution of $CO_2$ to the total

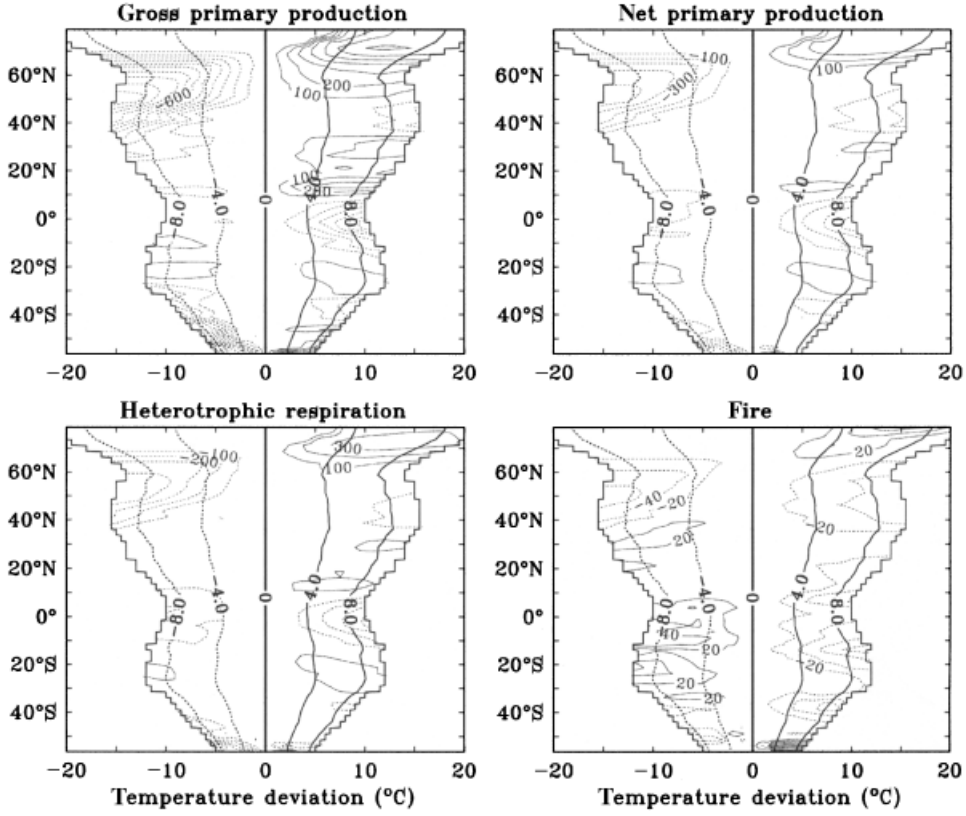


**Fig. 7** As Figs 4 and 6, but for deviations in zonally averaged carbon fluxes in $g\,C\,yr^{-1}\,m^{-2}$.

radiative forcing, $\Delta T_\gamma$ as a function of $CO_2$ and $\Delta T_{glob}$:

$$\Delta T_\gamma \equiv \Delta T_{2x}\left[\frac{RF(CO_2)}{RF(all)}\right]^{-1} = \Delta T_{glob}\cdot RF(2xCO_{2,0})\cdot[RF(CO_2)]^{-1}. \quad (4)$$

RF(all) is taken to be the sum of global mean radiative forcing from all greenhouse gases and from aerosols, whereas the EOF patterns (Fig. 1) of the climate substitute model were determined from a $CO_2$ only simulation. This approximation seems justified because the correlation between the fields obtained from greenhouse gas only simulations and from simulations with greenhouse gases and aerosols for a distinct Atmosphere Ocean General Circulation Model (AOGCM) is, in general, higher than the correlation between output fields obtained with different AOGCMs (Cubasch *et al*., 2001).

The modified climate sensitivity $\Delta T_\gamma$ has been evaluated from Eqn (4) for each of our 246 simulations and the global ECSC has been plotted as a function of $CO_2$ and $\Delta T_\gamma$ (Fig. 8, upper panel). For $CO_2$ levels above the preindustrial reference of 280 ppm, the global ECSC increases with $CO_2$ for $\Delta T_\gamma$ of less than 5 °C. For larger changes in $\Delta T_\gamma$, the ECSC tends to become smaller with increasing $CO_2$ in response to the related strong increase in temperature. For $CO_2$ below 280 ppm, simulated global ECSC does only weakly depend on $\Delta T_\gamma$ and decreases with $CO_2$. Figure 8 (upper panel) also illustrates that terrestrial carbon storage becomes smaller with a higher contribution of non-$CO_2$ radiative forcing to the total forcing, as found earlier (Joos *et al*., 2001).

A potential terrestrial uptake associated with increasing atmospheric $CO_2$ may in principal be limited by nutrient availability (Oren *et al*., 2001; Finzi *et al*., 2002), a feature not included in the model. Carbon to nitrogen ratios in terrestrial organic matter vary over more than two orders of magnitude (McGuire *et al*., 1992) and the inputs of reactive nitrogen to ecosystems in the absence of pollution, through $N_2$ fixation and N deposition derived from $NO_x$ production by soil processes and fires in nonlocal ecosystems, remain relatively poorly quantified (Cleveland *et al*., 1999; Vitousek & Field, 2001; Perakis & Hedin, 2002). These problems make it difficult to estimate nitrogen demand for additional carbon storage and to assess the impact of a potential nitrogen limitation on carbon storage. The change in nitrogen demand has been estimated for all experiments by applying a carbon to nitrogen ratio of 200 : 1

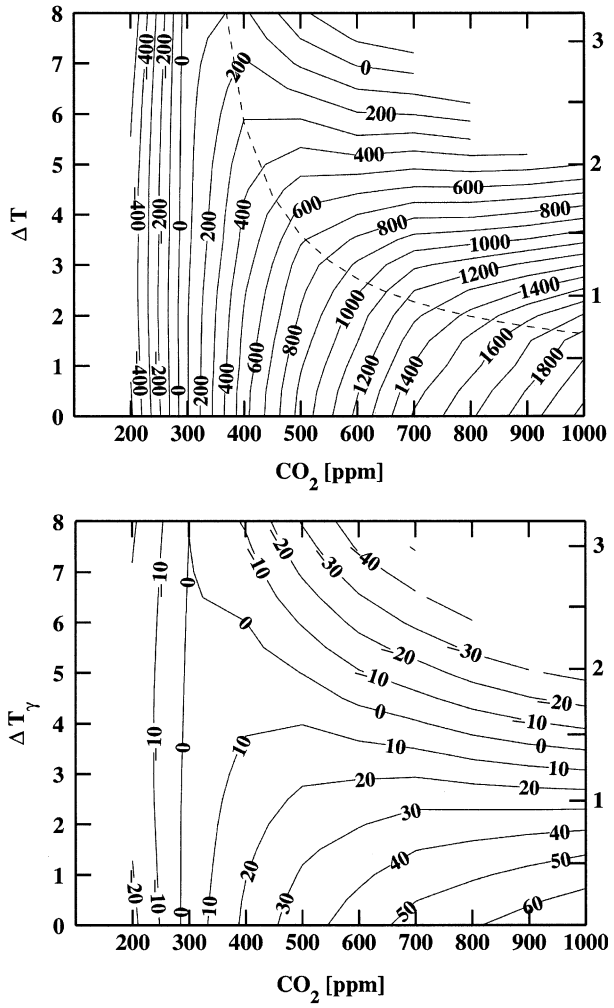


**Fig. 8** Simulated changes in terrestrial carbon stocks (Gt C, top) and nitrogen requirements (Gt N, bottom) as a function of atmospheric $CO_2$ and the modified climate sensitivity $\Delta T_\gamma$. The modified climate sensitivity (left-hand *y*-axis) is the climate sensitivity for a nominal doubling of $CO_2$ divided by the fraction of radiative forcing by $CO_2$ to the total radiative forcing. The reciprocal of this fraction is shown on the right-hand *y*-axis for a constant climate sensitivity of 2.5 °C. Moving vertically upward in the figure corresponds to an increase in non-$CO_2$ forcing for a constant climate sensitivity or to an increase in the climate sensitivity for a constant fraction of non-$CO_2$ forcing of the total forcing. Nitrogen requirements are calculated using a constant N/C ratio for vegetation (1/200) and for soils (1/15). The dashed line in the top panel indicates a global mean temperature deviation of 3 °C.

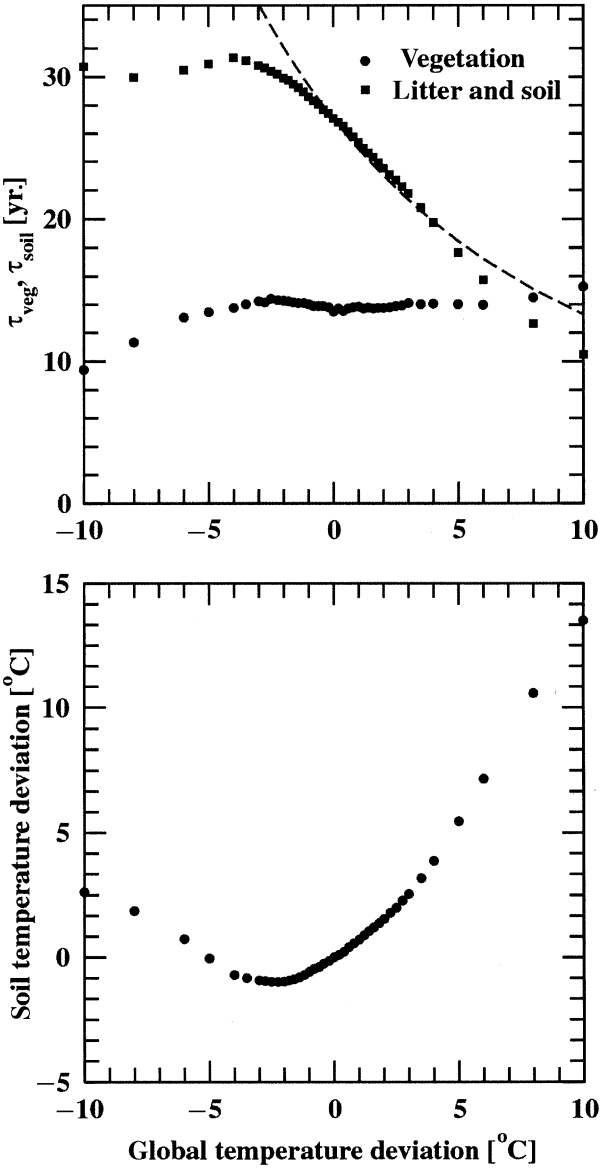


**Fig. 9** Global average soil temperature (bottom) and global average turnover time τ of the carbon stored in vegetation and in the combined litter and soil carbon pools (top) as a function of the global average surface temperature perturbation. Turnover times are from Lund–Potsdam–Jena simulations with $CO_2$ set to 280 ppm (symbols) and calculated by dividing the global vegetation carbon inventory, and the global litter and soil carbon inventory by the global net primary productivity. Soil temperature is calculated using Eqn (5). An exponential relationship ($\tau = c \exp[+308/(61.02 + \Delta T_{glob})]$) between soil turnover and global average temperature as typically applied in global box models (e.g. Lenton & Huntingford, 2003) is shown for comparison (dash).

for vegetation pools (leaves, fine roots, sapwood, and heartwood) and 15:1 for all litter and soil pools (Hungate *et al.*, 2003). Nitrogen storage varies between −20 and 60 Gt N, whereas the global ECSC varies between −500 and 2000 Gt C relative to the preindustrial state (Fig. 8). Global nitrogen demand is modest or negative if the modified climate sensitivity, $\Delta T_\gamma$ is larger than 3 °C. Global nitrogen demand becomes high if the climate sensitivity is below the accepted lower limit of 1.5 °C. Our illustrative calculation suggests that nitrogen limitation becomes potentially most important

for high $CO_2$ concentrations in combination with low warming (or cooling).

The above calculation is highly simplified and does not take into account a potential change in C : N ratios (Norby & Cotrufo, 1998; Van Kessel *et al*., 2000; Gill *et al*., 2002) or changes in the allocation of carbon to different compartments (McMurtrie *et al*., 2001; Schlesinger & Lichter, 2001). For example, Gill *et al.* (2002) find a significant increase in the C : N ratio of leaves, crowns, root, soil organic matter, and soil particulate matter together with an increase in NPP along a $CO_2$ gradient from 200 to 550 ppm in a grassland study. Such an increase as found in the field, in particular in soil C : N ratios, would lower the necessary nitrogen demand to support higher than present carbon storage. This would also bring into agreement estimates of nitrogen supply (Hungate *et al*., 2003) and the nitrogen required to support estimated terrestrial storage for the range of the Intergovernmental Panel on Climate Change (IPCC) emission scenarios (Joos *et al*., 2001; Prentice *et al*., 2001).

### *Global mean turnover rates and simple box models*

Soil and litter decomposition rates are important controls on the ECSC as most of the terrestrial organic carbon is stored in soils. Litter and soil organic matter decomposition rates are assumed to depend on global average surface temperature in several published global box models (Sarmiento *et al*., 1995; Meyer *et al*., 1999; Kheshgi & Jain, 2003; Lenton & Huntingford, 2003). In contrast, in the LPJ-DGVM decomposition rates through RH and fire depend on local temperatures and soil moisture. Hence, the global average decomposition rate reflects the distribution of soil and litter carbon in the climate space. Next, we investigate to which extent the box-model assumption that global average surface temperature governs soil organic carbon turnover is compatible with the LPJ-DGVM results.

First, we evaluate global average turnover of soil and litter organic carbon (Fig. 9). The turnover rate is the inverse of the average decomposition rate and corresponds at equilibrium to the mean residence time of carbon in a pool (Bolin & Rodhe, 1973). Global soil turnover, $\tau_{\mathrm{soil,glob}}$ is calculated by dividing the global soil and litter organic matter inventory by its throughput. The throughput equals the global NPP, i.e. the total flux entering the soil and litter reservoirs, or the combined RH and fire fluxes (i.e. the global flux leaving the soil and litter reservoirs). $\tau_{\mathrm{soil,glob}}$ depends almost linearly on the global average surface temperature deviation for $\Delta T_{\mathrm{glob}}$ above $-2\,^{\circ}\mathrm{C}$. However, $\tau_{\mathrm{soil,glob}}$ remains almost constant for lower $\Delta T_{\mathrm{glob}}$ and associated changes in local temperature, precipitation, and cloud cover. The dependency of soil organic carbon turnover as typically assumed in global box model is shown for comparison in Fig. 9. The box-model assumption that global soil organic carbon turnover depends roughly exponentially on global surface temperature (Sarmiento *et al*., 1995; Meyer *et al*., 1999; Kheshgi & Jain, 2003; Lenton & Huntingford, 2003) holds only over a limited temperature range. This finding does not necessarily invalidate earlier conclusions obtained by applying this class of box models. In particular, the temperature dependence of soil turnover is compatible with the LPJ results for the temperature range found in typical IPCC global-warming scenarios.

The climate dependence of soil organic matter turnover is further analyzed by investigating soil temperatures. An effective global average soil temperature, $T_{\mathrm{soil,glob}}$, is calculated from local soil temperatures and using local soil (including litter) organic matter inventories, SOM($x$), as weights:

$$T_{\mathrm{soil,glob}} = \sum_x T_{\mathrm{soil}}(x)\,\frac{\mathrm{SOM}(x)}{\sum_x \mathrm{SOM}(x)}. \qquad (5)$$

The global soil temperature deviation depends highly nonlinear on the global average surface temperature deviation (Fig. 9). In particular, the global soil temperature increases with decreasing global temperature for $\Delta T_{\mathrm{glob}}$ below $-3\,^{\circ}\mathrm{C}$. The reason is that under cold climate regimes a larger fraction of the total soil and litter carbon is stored in the tropics and in midlatitudes (Fig. 6), partly owing to high-latitude forest dieback. Shifts in the location of production lead to a situation where the litter and soil carbon pools experience, on average, a warmer climate, even when global mean temperature decreases. The consequence is that soil turnover remains nearly constant for $\Delta T_{\mathrm{glob}}$ below $-2\,^{\circ}\mathrm{C}$.

## Discussion and conclusions

The LPJ-DGVM has been run to equilibrium for a range of different climate states and atmospheric $CO_2$ concentrations. Local deviations in temperature, precipitation, and cloud cover are obtained by scaling spatial perturbation patterns with global average surface temperature deviations. This highly idealized setting allows us to simulate the first-order dependency of the ECSC and vegetation distribution on climate change.

Simulated production and terrestrial carbon inventories show a strong response to increasing atmospheric $CO_2$, yet the sensitivity to $CO_2$ variations decreases with increasing $CO_2$. The response of the terrestrial biosphere to increasing $CO_2$ may further be limited by

nutrient availability (Hungate *et al.*, 2003), a mechanism not explicitly modeled in LPJ. On the other hand, increasing rates of RH in cold climates may promote increased productivity by increasing nitrogen mineralization rates, thus alleviating nitrogen limitation, and by shifting productivity towards more woody plants with higher C : N ratios (e.g. Melillo *et al.*, 1993; Rastetter *et al.*, 1997; Medlyn *et al.*, 2000; Rastetter *et al.*, 2003).

In the absence of $CO_2$ fertilization, the modeled global ECSC shows a weak sensitivity to climate change for modest warming or cooling. This is compatible with small century scale changes in atmospheric $CO_2$ of a few parts per million only during the past millennium and the Holocene (Indermühle *et al.*, 1999; Gerber *et al.*, 2003; Joos & Prentice, 2004). However, ECSC decreases strongly with warming for global surface temperature deviations above $\sim 3\,^{\circ}C$, a value reached by the end of the century for midrange greenhouse gas emission scenarios (Houghton *et al.*, 2001).

Global warming leads to a pronounced poleward spreading of tropical, temperate, and boreal trees. This is compatible with available proxy data for the mid-Holocene (Prentice *et al.*, 2000; Bigelow *et al.*, 2003; Kaplan *et al.*, 2003). The biome distributions simulated by LPJ for mid-Holocene and Last Glacial Maximum (LGM) conditions have been found to be comparable with vegetation reconstructions based on pollen and plant macrofossil data in an earlier study (Joos *et al.*, 2004).

Our results can be used to improve existing terrestrial box models. A nonlinear threshold behavior is found for the sensitivity of carbon storage to climate change. The loss rate of carbon to the atmosphere per unit change in global average surface temperature is predicted to double when a threshold of $\sim 3\,^{\circ}C$ is crossed. This nonlinearity is coupled to regional changes in plant distribution and productivity.

Changes in plant distribution such as the poleward spreading of trees with warming have an important impact on the global average soil decomposition rate. The global average turnover time of soil and litter carbon increases with warming under cool climate conditions to reach a maximum and then decreases for warmer climate. This finding conflicts with the assumption made in several published global terrestrial box models (Sarmiento *et al.*, 1995; Meyer *et al.*, 1999; Kheshgi & Jain, 2003; Lenton & Huntingford, 2003) that soil decomposition rates depend exponentially on global average surface temperature. This limitation of global box models could be overcome by considering latitudinal variations in their setup.

This study, with its focus on equilibrium responses, complements the earlier work on transients. The transient response behavior of LPJ to changes in climate has been studied in the context of multimillennial changes over the past 20 000 years (Kaplan *et al.*, 2002; Joos *et al.*, 2004), decadal to century scale changes over the past millennium (Gerber *et al.*, 2003), the Younger Dryas cold period (Scholze *et al.*, 2003), and the industrial period (McGuire *et al.*, 2001; Joos *et al.*, 2001; Dargaville *et al.*, 2002), and for projected future climate perturbations (Joos *et al.*, 2001). Typical adjustment times of ECSC to a sudden perturbation in climate (and related atmospheric $CO_2$ changes) are a few decades for the main response (Gerber *et al.*, 2003), whereas it takes centuries to bring the slowly overturning soil pools into equilibrium. This is consistent with the analysis of soil radiocarbon data (Trumbore *et al.*, 1996; Perruchoud *et al.*, 1999).

The pathways towards equilibrium can be different and depend on rates of changes in climate and $CO_2$. High greenhouse gas emissions and high contributions of non-$CO_2$ agents to radiative forcing favor a transient terrestrial carbon source by enhancing warming and the associated release of soil carbon in simulations with LPJ (Joos *et al.*, 2001). Experimental work (Oechel *et al.*, 2000) suggests that warming results in immediate release of soil and litter carbon, because of increased decomposition rates by heterotrophs; but delayed plant responses, possibly associated with increases in nitrogen availability, may mitigate the initial carbon loss.

Results presented need to be interpreted cautiously in the view of various uncertainties. Different DGVMs forced by the same climate and $CO_2$ trajectories (Cramer *et al.*, 2001) or coupled to different climate models (Cox *et al.*, 2000; Joos *et al.*, 2001) yield different results for projected terrestrial carbon storage and changes in vegetation distribution. Different bounding assumption about the dependence of soil respiration on global warming and on the strength of $CO_2$ fertilization yield uncertainties in projected atmospheric $CO_2$ of $-10$ to $+20\%$ and in global average surface temperature of $-0.2$ to $+0.5\,^{\circ}C$ by year 2100 for a range of IPCC scenarios (Joos *et al.*, 2001). Uncertainties in terrestrial carbon storage are related to uncertainties (1) in the pattern of climate change, (2) in the response of the land biosphere to climate change, and (3) in the response to atmospheric $CO_2$. Further, anthropogenic land use change, another important driver for terrestrial C storage, is not taken into account in this study.

Shortcomings of the pattern scaling approach are many, for example, that potential changes in the frequency and magnitude of extreme climate events (Schär *et al.*, 2004), of climate modes such as the El Niño Southern Oscillation or the North Atlantic Oscillation, and changes in ice sheet extent and sea level are not considered. Similarly, feedbacks between changes in

vegetation and associated changes in surface albedo, roughness and evapotranspiration, and climate are neglected. For example, such feedbacks are important to correctly model the reduction of the Sahara desert (de Noblet-Ducoudré *et al*., 2000) as reconstructed for mid-Holocene conditions (Jolly *et al*., 1998). The spatio-temporal patterns of climate change depend on the type of forcing. However, the climatic response to solar, greenhouse gas, and anthropogenic aerosol forcing is primarily governed by the characteristics of the applied AOGCM and to a smaller degree by the type of forcing (Cubasch *et al*., 2001). The climate response patterns for volcanic forcing show, in general, cooling, but show for Northern Hemisphere winter time warming. Observation-derived patterns have been used to describe the climate response to explosive volcanic eruptions in earlier work with LPJ (Gerber *et al*., 2003). The temperature pattern obtained from ECHAM3/LSG exhibits the typical structure (i.e. above-average warming in high northern latitudes and in the interiors of the Northern Hemisphere continents) found in the state-of-the-art AOGCMs (Covey *et al*., 2000; Meehl *et al*., 2000; Cubasch *et al*., 2001) forced with increasing greenhouse gas and anthropogenic aerosol concentrations. Uncertainties in precipitation patterns are large and different AOGCM yield qualitatively different results (Cubasch *et al*., 2001). Some AOGCMs (e.g. the Hadley Centre model) yield drier conditions in the Amazon region under global warming, in contrast to the ECHAM3/LSG results. The resulting drought stress caused dieback of extant forests in DGVM simulations with climate input from the Hadley model (White *et al*., 2000) or in coupled AOGCM–DGVM simulations (Cox *et al*., 2000).

We compare results of this study with results from previous equilibrium simulations for LGM boundary conditions (Joos *et al*., 2004) to further investigate the implications of our simplified setup. LPJ-DGVM was forced by precipitation and climate anomalies obtained from a simulation with the state-of-the-art Climate System Model of the National Center for Atmospheric Research in which greenhouse gas concentrations, ice sheet extent, and orbital forcing were prescribed from paleoreconstructions (Shin *et al*., 2002). Then, global carbon storage in vegetation, litter, soil, and global fluxes (crosses in Figs 2 and 3) are similar to those with the pattern scaling approach. The simulated increase in ECSC of 850 Gt C since the LGM is compatible with data-based reconstructions and their uncertainties as discussed elsewhere (Joos *et al*., 2004).

The acclimation of terrestrial biological processes to changed environmental conditions is crucial for the long-term dynamics of the biosphere. Acclimation occurs at several levels. For example, the adjustment of plant-type composition and distribution to climate change, as modeled in DGVMs, is a key homeostatic mechanism for the biosphere as a whole. More subtle acclimation processes act through physiological adjustments within individual plants. Key physiological acclimation processes are modeled, implicitly or explicitly, by LPJ-DGVM. GPP is not assumed to have a fixed temperature optimum but rather adapts to changing environmental conditions on a seasonal basis, consistent with FLUXNET observations (Baldocchi *et al*., 2001). Photosynthetic capacity and leaf nitrogen content also adjust implicitly to changes in temperature, light availability and ambient atmospheric $CO_2$ concentration (Haxeltine & Prentice, 1996b; Prentice, 2001), resulting in downregulation of carboxylation capacity as $CO_2$ increases and homeostasis of carboxylation capacity along temperature gradients. The apparent acclimation of soil RH to temperature over 1 to 3 years as seen in soil warming experiments (Jarvis & Linder, 2000; Rustad *et al*., 2001) can be explained by a rapid re-equilibration of labile carbon pools which account for most of the measured $CO_2$ efflux over a time scale too short to allow measurable decay of the slower soil fractions (Prentice *et al*., 2004). The apparent temperature insensitivity of annual carbon loss in incubation experiments (Giardina & Ryan, 2000), similarly, is expected given the heterogeneity of turnover times in soil organic matter (Prentice *et al*., 2004). These observations have little direct bearing on ECSC and they are fully consistent with the predictions of multicompartment soil carbon models, including the relatively simple model (Foley, 1995) embedded in LPJ-DGVM. Nevertheless, there is considerable scope for systematic comparisons of DGVM predictions with experiments and observations in order to evaluate and improve the models' simulation of carbon cycling processes at the whole-ecosystem level.

The extent of stimulation of carbon storage in natural ecosystems by $CO_2$ has been a matter of controversy (Hättenschwiler *et al*., 1997; Luo *et al*., 1999). There is a debate whether the current terrestrial sink of order 10–20 Gt C per decade (Prentice *et al*., 2001) is indeed due to $CO_2$ fertilization as suggested by terrestrial models (McGuire *et al*., 2001). Other processes, such as nitrogen fertilization (Schindler & Bayley, 1993; Townsend *et al*., 1996), climate variations (McGuire *et al*. 2001), and forest regrowth (Caspersen *et al*., 2000; Joos *et al*., 2002) might, in principle, be responsible for part or most of the present terrestrial sink. It is also questioned whether the $CO_2$ fertilization mechanism will continue to operate under the projected $CO_2$ increase or whether plant acclimation and nitrogen and other nutrient limitations inhibit further $CO_2$-driven carbon uptake (Cowling & Field, 2003; Hungate *et al*., 2003). A role for

$CO_2$ fertilization in determining terrestrial carbon storage at concentrations within the glacial–interglacial range (180–280 ppm) has support from a range of data-based studies (Peng *et al*., 1998; Bennett & Willis, 2000; Cowling & Field, 2003; Harrison & Prentice, 2003; Midgley *et al*., 2003). The magnitude of the $CO_2$ fertilization response in LPJ is consistent with the recent amplification of the seasonal cycle in atmospheric $CO_2$ (McGuire *et al*. 2001; Dargaville *et al*., 2002) and with the enhancement of NPP shown in free air carbon dioxide enrichment experiments (DeLucia *et al*., 1999; T. Hickler, unpublished results).

Although there is still considerable uncertainty about the relative magnitude of fundamental ecosystem processes, paleodata clearly indicate that terrestrial carbon storage and biome distribution have varied under different climatic regimes (Shackleton, 1977; Cooperative Holocene Mapping Project Members, 1988; Bird *et al*., 1994; Crowley, 1995; Jolly *et al*., 1998; Bigelow *et al*., 2003; Harrison & Prentice, 2003). This study represents a first attempt to use a state-of-the-art DGVM to explore the variations of potential terrestrial carbon storage in a parameter space determined by $CO_2$ and the climate changes linked to changing $CO_2$. The robustness and realism of the conclusions should be assessed through the comparison of different formulations of fundamental processes (particularly regarding the interaction of carbon and nitrogen cycles) and through comparisons of model results with observational and experimental data that test the correctness of the model formulations across the widest possible range of conditions.

## Acknowledgements

This work is funded by the Swiss National Science foundation.

## References

Baldocchi D, Falge E, Gu L *et al*. (2001) FLUXNET: a new tool to study the temporal and spatial variability of ecosystem-scale carbon dioxide, water vapor, and energy flux density. *Bulletin of the American Meteorological Society*, **82**, 2415–2434.

Bennett KD, Willis KJ (2000) Effect of global atmospheric carbon dioxide on glacial–interglacial vegetation change. *Global Ecology and Biogeography*, **9**, 355–361.

Bigelow NH, Brubaker LB, Edwards ME *et al*. (2003) Climate change and Arctic ecosystems: 1. vegetation changes north of 55°N between the Last Glacial Maximum, mid-Holocene and present. *Journal of Geophysical Research*, **180**, doi 10.1029/2002JD002,558.

Bird MI, Lloyd J, Farquhar GD (1994) Terrestrial carbon storage at the LGM. *Nature*, **371**, 566.

Bolin B, Rodhe H (1973) A note on the concepts of age distribution and transit time in natural reservoirs. *Tellus*, **25**, 58–62.

Cao M, Woodward FI (1998) Dynamic responses of terrestrial ecosystem carbon cycling on global climate change. *Nature*, **393**, 249–251.

Caspersen JP, Pacla SW, Jenkins JC *et al*. (2000) Contributions of land-use history to carbon accumulation in U.S. forests. *Science*, **290**, 1148–1151.

Collatz GJ, Ribas-Carbo M, Berry JA (1992) A coupled photosynthesis – stomatal conductance model for leaves of $C_4$ plants. *Australian Journal of Plant Physiology*, **19**, 519–538.

Cleveland CC, Townsend AR, Schimel DS *et al*. (1999) Global patterns of terrestrial biological nitrogen (N-2) fixation in natural ecosystems. *Global Biogeochemical Cycles*, **13**, 623–645.

Cooperative Holocene Mapping Project Members (1988) Climate changes of the last 18'000 years: observations and model simulations. *Science*, **241**, 1043–1052.

Cox PM, Betts RA, Jones CD *et al*. (2000) Acceleration of global warming due to carbon-cycle feedbacks in a coupled climate model. *Nature*, **408**, 184–187.

Covey C, Achuta Rao KM, Lambert SJ *et al*. (2000) *Intercomparison of present and future climates simulated by coupled ocean–atmosphere GCMs*, PCMDI Report No. 66, Program for Climate Model Diagnosis and Intercomparison, Lawrence Livermore National Laboratory, University of California, Livermore, CA.

Cowling SA, Field CB (2003) Environmental control of leaf area production: implications for vegetation and land–surface modeling. *Global Biogeochemical Cycles*, **17**, doi:10.1029/2002GB001,915.

Cramer W, Bondeau A, Woodward FI *et al*. (2001) Global response of terrestrial ecosystem structure and function to $CO_2$ and climate change: results from six global dynamic vegetation models. *Global Change Biology*, **7**, 357–373.

Crowley TJ (1995) Ice age terrestrial carbon changes revisited. *Global Biogeochemical Cycles*, **9**, 377–389.

Cubasch U, Meehl GA, Boer GJ *et al*. (2001) Projections of future climate change. In: *Climate Change 2001: The Scientific Basis. Contribution of Working Group I to the Third Assessment Report of the Intergovernmental Panel on Climate Change* (eds Houghton JT, Ding Y, Griggs D, Noguer M, van der Linden P, Dai X, Maskell K, Johnson CA), pp. 525–582. Cambridge University Press, Cambridge, UK and New York, NY, USA.

Cubasch U, Santer BD, Hegerl GC (1995) Klimamodelle – wo stehen wir ? *Physikalische Blätter*, **51**, 269–276.

Dargaville RJ, Heimann M, McGuire A.D. *et al*. (2002) Evaluation of terrestrial carbon cycle models with atmospheric $CO_2$ measurements: results from transient simulations considering increasing $CO_2$, climate, and land-use effects. *Global Biogeochemical Cycles*, **16**, doi: 10.1029/2001GB001,426.

DeLucia EH, Hamilton JG, Naidu SL *et al*. (1999) Net primary production of a forest ecosystem with experimental $CO_2$ enrichment. *Nature*, **284**, 1177–1179.

de Noblet-Ducoudré N, Claussen M, Prentice IC (2000) Mid-Holocene greening of the Sahara: first results of the GAIM 6000 year BP experiment with two asynchronously coupled atmosphere/biome models. *Climate Dynamics*, **6**, 643–659.

Farquhar GD, von Caemmerer S, Berry JA (1980) A biochemical model of photosynthetic $CO_2$ assimilation in leaves of $C_3$ species. *Planta*, **149**, 78–90.

Finzi AC, DeLucia EH, Hamilton JG *et al*. (2002) The nitrogen budget of a pine forest under free air $CO_2$ enrichment. *Oecologia*, **132**, 567–578.

Foley JA (1995) An equilibrium model of the terrestrial carbon budget. *Tellus*, **47B**, 310–319.

Friedlingstein P, Bopp L, Ciais P *et al*. (2001) Positive feedback between future climate change and the carbon cycle. *Geophysical Research Letters*, **28**, 1543–1547.

Gerber S, Joos F, Brügger P *et al*. (2003) Constraining temperature variations over the last millennium by comparing simulated and observed atmospheric $CO_2$. *Climate Dynamics*, **20**, 281–299 (doi:10.1007/s00382-002-0270-8).

Giardina C, Ryan M (2000) Evidence that decomposition rates of organic carbon in mineral soil do not vary with temperature. *Nature*, **404**, 858–861.

Gill RA, Polley HW, Johnson HB *et al*. (2002) Nonlinear grassland responses to past and future atmospheric $CO_2$. *Nature*, **417**, 279–282.

Harrison SP, Prentice IC (2003) Climate and $CO_2$ controls on global vegetation distribution at the Last Glacial Maximum: analysis based on palaeovegetation data, biome modeling and palaeoclimate simulation. *Global Change Biology*, **9**, 983–1004.

Hättenschwiler S, Miglietta F, Raschi M *et al*. (1997) Thirty years of *in situ* tree growth under elevated $CO_2$: a model for future forest responses. *Global Change Biology*, **3**, 463–471.

Haxeltine A, Prentice IC (1996a) BIOME 3: an equilibrium terrestrial biosphere model based on ecophysiological constraints, resource availability and competition among plant functional types. *Global Biogeochemical Cycles*, **10**, 693–703.

Haxeltine A, Prentice IC (1996b) A general model for the light-use efficiency of primary productivity. *Functional Ecology*, **10**, 551–561.

Hooss G, Voss R, Hasselmann K *et al*. (1999) *A nonlinear impulse response model of the coupled carbon cycle–ocean–atmosphere climate system*. Max-Planck-Institut für Meteorologie, Hamburg, Technical Report No. 290.

Hooss G., Voss R, Hasselmann K *et al*. (2001) A non-linear impulse response model of the coupled carbon cycle–ocean–atmosphere climate system (NICCS). *Climate Dynamics*, **18**, 189–202.

Houghton JT, Ding Y, Griggs D, Noguer M, van der Linden P, Dai X, Maskell K, Johnson C, eds (2001) *Climate Change 2001: The Scientific Basis, Intergovernmental Panel on Climate Change*. Cambridge University Press, Cambridge, UK.

Hungate BA, Dukes JS, Shaw MR *et al*. (2003) Nitrogen and climate change. *Science*, **302**, 1512–1513.

Indermühle A, Stocker TF, Joos F *et al*. (1999) Holocene carbon–cycle dynamics based on $CO_2$ trapped in ice at Taylor Dome, Antarctica. *Nature*, **398**, 121–126.

Jarvis P, Linder S (2000) Botany – Constraints to growth of boreal forests. *Nature*, **405**, 904–905.

Johns T, Carnell R, Crossley J *et al*. (1997) The second Hadley Centre coupled ocean–atmosphere GCM: model description, spinup and validation. *Climate Dynamics*, **13**, 103–134.

Jolly D, Prentice IC, Bonnefille R *et al*. (1998) Biome reconstruction from pollen and plant macrofossil data for Africa and the Arabian peninsula at 0 and 6000 years. *Journal of Biogeography*, **25**, 1007–1027.

Joos F, Gerber S, Prentice IC *et al*. (2004) Transient simulations of Holocene atmospheric carbon dioxide and terrestrial carbon storage since the Last Glacial Maximum. *Global Biogeochemical Cycles*, **18**, doi:10.1029/2003GB002156.

Joos F, Prentice IC (2004) Chapter: A paleo-perspective on changes in atmospheric $CO_2$ and climate. In: *The Global Carbon Cycle Integrating Humans, Climate and the Natural World* (eds Field CB & Raupach HR). SCOPE 62, Island Press.

Joos F, Prentice IC, House JI (2002) Growth Enhancement due to Global Atmospheric Change as Predicted by Terrestrial Ecosystem Models: consistent with U.S. Forest Inventory Data. *Global Change Biology*, **8**, 299–303.

Joos F, Prentice IC, Sitch S *et al*. (2001) Global warming feedbacks on terrestrial carbon uptake under the Intergovernmental Panel on Climate Change (IPCC) emission scenarios. *Global Biogeochemical Cycles*, **15**, 891–907.

Kaplan JO, Bigelow NH, Prentice IC *et al*. (2003) Climate change and arctic ecosystems II: modeling, paleodata-model comparisons, and future projections. *Journal of Geophysical Research – Atmosphere*, **108**, 8171 (doi: 10.1029/2002JD002559).

Kaplan JO, Prentice IC, Knorr W *et al*. (2002) Modeling the dynamics of terrestrial carbon storage since the Last Glacial Maximum. *Geophysical Research Letters*, **29**, doi: 10.1029/2001GL015230.

Kheshgi HS, Jain AK (2003) Projecting future climate change: implications of carbon cycle model intercomparisons. *Global Biogeochemical Cycles*, **17**, doi:10.1029/2001GB001842.

Leemans R, Cramer WP (1991) *The IIASA climate database for land areas on a grid with 0.5° resolution*. Research report rr -91-18, Technical report, International Institute for Applied System Analysis

Leemans R, Eickhout B, Strengers B *et al*. (2002) The consequences for the terrestrial carbon cycle of uncertainties in land use, climate and vegetation responses in the IPCC SRES scenarios. *Science in China Series C – Life Sciences*, **45**, 126.

Lenton TM, Huntingford C (2003) Global terrestrial carbon storage and uncertainties in its temperature sensitivity examined with a simple model. *Global Change Biology*, **9**, 1333–1352.

Lloyd J, Taylor JA (1994) On the temperature dependence of soil respiration. *Functional Ecology*, **8**, 315–323.

Luo Y, Reynolds J, Wang Y (1999) A search for predictive understanding of plant responses to elevated $CO_2$. *Global Change Biology*, **5**, 143–156.

McGuire AD, Melillo JM, Joyce LA *et al*. (1992) Interactions between carbon and nitrogen dynamics in estimating net primary productivity for potential vegetation in North America. *Global Biogeochemical Cycles*, **6**, 101–124.

McGuire AD, Sitch S, Clein JS *et al*. (2001) Carbon balance of the terrestrial biosphere in the twentieth century: analysis of $CO_2$, climate and land-use effects with four process-based ecosystem models. *Global Biogeochemical Cycles*, **15**, 183–206.

McMurtrie RE, Medlyn BE, Dewar RC (2001) Increased understanding of nutrient immobilization in soil organic matter is critical for predicting the carbon sink strength of forest ecosystems over the next 100 years. *Tree Physiology*, **21**, 831–839.

Medlyn BE, McMurtrie RE, Dewar RC *et al*. (2000) Soil processes dominate the long-term response of forest net primary

productivity to increased temperature and atmospheric $CO_2$ concentration. *Canadian Journal of Forest Research*, **30**, 873–888.

Meehl GA, Boer GJ, Covey C *et al*. (2000) The Coupled Model Intercomparison Project (CMIP). *Bulletin of the American Meteorological Society*, **81**, 313–318.

Melillo JM, McGuire AD, Kicklighter DW *et al*. (1993) Global climate change and terrestrial net primary production. *Nature*, **363**, 234–240.

Meyer R, Joos F, Esser G *et al*. (1999) The substitution of high-resolution terrestrial biosphere models and carbon sequestration in response to changing $CO_2$ and climate. *Global Biogeochemical Cycles*, **13**, 785–802.

Midgley GF, Aranibar JN, Mantlana KB *et al*. (2003) Photosynthetic and gas exchange characteristics of dominant woody plants on a moisture gradient in an African savanna. *Global Change Biology*, **10**, 309–317.

Monteith JL (1995) Accommodation between transpiring vegetation and the convective boundary layer. *Journal of Hydrology*, **166**, 251–263.

Myhre G, Highwood EJ, Shine K *et al*. (1998) New estimates of radiative forcing due to well mixed greenhouse gases. *Geophysical Research Letters*, **25**, 2715–2718.

Norby RJ, Cotrufo MF (1998) A question of litter quality. *Nature*, **396**, 17–18.

Oechel WC, Vourlitis GL, Hastings SJ *et al*. (2000) Acclimation of ecosystem $CO_2$ exchange in the Alaskan Arctic in response to decadal climate warming. *Nature*, **406**, 978–981.

Oren R, Ellsworth DS, Johnsen KH *et al*. (2001) Soil fertility limits carbon sequestration by forest ecosystem in a $CO_2$ enriched atmosphere. *Nature*, **411**, 469–472.

Peng CH, Guiot J, Van Campo E (1998) Estimating changes in terrestrial vegetation and carbon storage: using palaeoecological data and models. *Quaternary Science Reviews*, **17**, 719–735.

Perakis SS, Hedin LO (2002) Nitrogen loss from unpolluted South American forests mainly via dissolved organic compounds. *Nature*, **415**, 416–419.

Perruchoud D, Joos F, Fischlin A *et al*. (1999) Evaluating time scales of carbon turnover in temperate forest soils with radiocarbon data. *Global Biogeochemical Cycles*, **13**, 555–573.

Prentice IC (2001) Controls on the primary productivity of terrestrial ecosystems. Pages 873–874 in: Geider RJ, DeLucia EH, Falkowski PG *et al*. Primary productivity of planet earth: biological determinants and physical constraints in terrestrial and aquatic habitats. *Global Change Biology*, **7**, 849–882.

Prentice IC, Farquhar GD, Fasham MJ *et al*. (2001) The carbon cycle and atmospheric $CO_2$. In: *Climate Change 2001: The Scientific Basis. Contribution of Working Group I to the Third Assessment Report of the Intergovernmental Panel on Climate Change* (eds Houghton JT, Ding Y, Griggs D, Noguer M, van der Linden P, Dai X, Maskell K, Johnson CA), pp. 183–237. Cambridge University Press, Cambridge, UK and New York, NY, USA.

Prentice IC, Jolly DBIOME 6000 participants (2000) Mid-Holocene and glacial-maximum vegetation geography of the northern continents and Africa. *Journal of Biogeography*, **27**, 507–519.

Prentice IC, Le Quéré C, Buitenhuis ET *et al*. (2004) Biosphere Dynamics: Challenges for Earth System Models. In: *The State of the Planet: Frontiers and Challenges* (eds Hawkesworth CS, Sparks RSJ). American Geophysical Union, Washington, USA.

Ramaswamy V, Boucher O, Haigh J *et al*. (2001) Radiative forcing of climate change. In: *Climate Change 2001: The Scientific Basis. Contribution of Working Group I to the Third Assessment Report of the Intergovernmental Panel on Climate Change* (eds Houghton JT, Ding Y, Griggs D, Noguer M, van der Linden P, Dai X, Maskell K, Johnson CA), pp. 349–416. Cambridge University Press, Cambridge, UK and New York, NY, USA.

Rastetter EB, Aber JD, Peters DPC *et al*. (2003) Using mechanistic models to scale ecological processes across space and time. *Bioscience*, **53**, 68–76.

Rastetter EB, Agren GI, Shaver GR (1997) Response of N-limited ecosystems to increased $CO_2$: a balanced-nutrition, coupled-element-cycles model. *Ecological Applications*, **7**, 444–460.

Rustad LE, Campbell JL, Marion BM *et al*. (2001) A meta-analysis of the response of soil respiration, net nitrogen mineralization, and aboveground plant growth to experimental ecosystem warming. *Oecologia*, **126**, 543–562.

Sarmiento JL, Le Quéré C, Pacala SW (1995) Limiting future atmospheric carbon dioxide. *Global Biogeochemical Cycles*, **9**, 121–137.

Schär C, Vidale PL, Lüthi D *et al*. (2004) The role of increasing temperature variability in European summer heatwaves. *Nature*, **427**, 332–336.

Schindler DW, Bayley SE (1993) The biosphere as an increasing sink for atmospheric carbon: estimates from increased nitrogen deposition. *Global Biogeochemical Cycles*, **7**, 717–733.

Schlesinger WH, Lichter J (2001) Limited carbon storage in soil and litter of experimental forest plots under increased atmospheric $CO_2$. *Nature*, **411**, 466–469.

Scholze M, Knorr W, Heimann M (2003) Modelling terrestrial vegetation dynamics and carbon cycling for an abrupt climate change event. *The Holocene*, **13**, 319–326.

Shackleton NJ (1977) Carbon-13 *uvigerina*: tropical rainforest history and the equatorial Pacific carbonate dissolution cycles. In: *The Fate of Fossil Fuel $CO_2$ in the Ocean* (eds Andersen NR, Malahoff A), pp. 401–428. Plenum, New York.

Shin S, Liu Z, Otto-Bliesner B *et al*. (2002) A simulation of the Last Glacial Maximum climate using the NCAR-CCSM. *Climate Dynamics*, **20**, 127–151 (doi:10.1007/s00382-002-0260-x).

Sitch S, Smith B, Prentice IC *et al*. (2003) Evaluation of ecosystem dynamics, plant geography and terrestrial carbon cycling in the LPJ dynamic global vegetation model. *Global Change Biology*, **9**, 161–185.

Townsend AR, Braswell BH, Holland EA *et al*. (1996) Spatial and temporal patterns in terrestrial carbon storage due to the deposition of fossil fuel nitrogen. *Ecological Applications*, **6**, 806–814.

Thonicke K, Venevsky S, Sitch S *et al*. (2001) The role of fire disturbance for global vegetation dynamics: coupling fire into a dynamic global vegetation model. *Global Ecology and Biogeography*, **10**, 661–677.

Trumbore SE, Chadwick OA, Amundson R (1996) Rapid exchange between soil carbon and atmospheric carbon dioxide driven by temperature change. *Science*, **272**, 393–396.

Van Kessel C, Horwath WR, Hartwig U *et al*. (2000) Net soil carbon input under ambient and elevated $CO_2$ concentrations: isotopic evidence after 4 years. *Global Change Biology*, **6**, 435–444.

Voss R, Mikolajewicz U (1999) *Long-term climate changes due to increased $CO_2$ concentration in the coupled atmosphere-ocean general circulation model ECHAM3/LSG*, Tech. Rep. 298, Max-Planck Institut für Meteorologie, Hamburg,.

Vitousek PM, Field CB (2001) Input–output balances and nitrogen limitation in terrestrial ecosystems. In: *Global Biogeochemical Cycles in the Climate System* (eds Schulze ED, Schimel D, Prentice IC, Heimann M, Harrison SP, Holland EA, Lloyd J), pp. 217–225. Academic Press, San Diego.

White A, Cannell MR, Friend AD (2000) $CO_2$ stabilization, climate change and the terrestrial carbon sink. *Global Change Biology*, **6**, 817–833.